Brightness and polarization scattering functions of different natures of asbestos in the visible and near infrared domain

Jean-Baptiste Renard, Cedric Duee, Xavier Bourrat, Hubert Haas, Jérémy Surcin, Benoit Couté

Brightness and polarization scattering functions of different natures of asbestos in the visible and near infrared domain

Jean-Baptiste RENARD , Cédric DUEE , Xavier BOURRAT , Hubert HAAS , Jérémy SURCIN , Benoit COUTE

PII: S0022-4073(19)30967-7
DOI: https://doi.org/10.1016/j.jqsrt.2020.107159
Reference: JQSRT 107159

To appear in: *Journal of Quantitative Spectroscopy & Radiative Transfer*

Received date: 10 December 2019
Revised date: 3 March 2020
Accepted date: 8 June 2020

Please cite this article as: Jean-Baptiste RENARD , Cédric DUEE , Xavier BOURRAT , Hubert HAAS , Jérémy SURCIN , Benoit COUTE , Brightness and polarization scattering functions of different natures of asbestos in the visible and near infrared domain, *Journal of Quantitative Spectroscopy & Radiative Transfer* (2020), doi: https://doi.org/10.1016/j.jqsrt.2020.107159

HIGHLIGHTS

- First scattering functions of asbestos
- Low polarization with positive color effect from green to near infrared
- Strong variability of brightness scattering function for different asbestos
- Chrysotile is the darkest sample at scattering angle of 90°

Brightness and polarization scattering functions of different natures of asbestos in the visible and near infrared domain

Jean-Baptiste RENARD (1), Cédric DUEE (2), Xavier BOURRAT (3), Hubert HAAS (2), Jérémy SURCIN (1), Benoit COUTE (1)
(1) LPC2E-CNRS, 3A avenue de la recherche scientifique, F-45071 Orléans cedex 2, France
(2) BRGM, F-45000 Orléans, France
(3) BRGM, F-51100 Reims, France

Abstract. Asbestos refers to silicate minerals belonging to the serpentine group (chrysotile) and the amphibole group (crocidolite, amosite, tremolite-asbestos, anthophyllite-asbestos and actinolite-asbestos). Such materials have strong effect on health, and real-time instrumentation is on demand to detect asbestos. The current real-time techniques use only some aspects of the optical properties of asbestos, since the scattering properties (brightness and linear polarization scattering functions) of the various natures of asbestos has not been yet fully determined. We present here the brightness and linear polarization scattering functions for 6 natures of asbestos in the 425-1650 nm spectral domain obtained with the PROGRA2 instrument. Although the samples exhibit different shapes, the linear polarization values remain low, bell-shaped as usual for irregular particles, and close to those of mineral particles previously studied with PROGRA2. On the opposite, asbestos brightness curves present strong differences for the different samples. The chrysotile is darker than the other samples in the 80°-150° angle range, probably due to its tubular shape that can act as a light trap for scattering angles greater than a few tens of degrees. Other asbestos particles can be distinguished from building materials such as glass wool or plaster through their brightness curves in some scattering angle ranges. These new laboratory measurements indicate that the optical scattered properties could be used in the future to tentatively detect asbestos particles in a medium generated from building materials.

1. INTRODUCTION

Asbestos refers to several silicate minerals belonging to the serpentine group (chrysotile) and the amphibole group (crocidolite known as blue asbestos, anthophyllite-asbestos, amosite also called brown asbestos, tremolite-asbestos and actinolite-asbestos) [1,2]. Due to their interesting properties such as chemical, electrical, mechanical or heat resistance, these natural minerals have been widely used in constructions, for example, in France until its total ban in 1997. Despite this ban, a lot of asbestos is still present in French constructions nowadays, with 90 % of it being chrysotile and the rest being amosite and crocidolite. It is well known that asbestos has carcinogenic effect. The inhalation of asbestos fibers causes respiratory inflammation and diseases such as asbestosis, lung cancer or malignant mesothelioma [3]. The hazard occurs when asbestos fibers are released in air, due to material degradation or refection work, and can therefore be inhaled.

The current reference methods to detect airborne asbestos or asbestos in materials are based on Transmission Electron Microscopy (TEM). However, these methods are indirect detection methods, which induces a delay between the sampling on-site and the analysis at laboratory. This delay can reach up to 48 hours and therefore stops any intervention on-site

during this time. Moreover, the research of asbestos by TEM requires the respect of a cumbersome preparation method, the aim of this preparation being to eliminate most of the matrix, for example by calcination or acid attack.

It appears important to reflect on a technique able to give a real-time response, especially if people's health is on the line. Using the optical properties of asbestos could be a useful tool for its detection. Until now, some studies have focused on the optical properties of asbestos, more precisely on refraction indices and extinction [4,5] and light scattering [6-13]. Verkouteren and Wylie [4] studied optical properties of 103 samples in the tremolite-actinolite-ferro-actinolite series. They showed that there are some changes in refractive indices, birefringence and extinction angle between 26 and 32 % ferro-actinolite, which may be due to tschermakite substitution. In another study |5], they stated that in most cases, refractive indices are predictable and can be used for identification of fibrous amphibole, as opposed to the extinction angle. Bandli et al. [14] studied samples of winchite, an amphibole, and showed that the refractive index and birefringence were dependent on the Mg content, but also that birefringence and particle morphology were correlated. Timbrell [6] showed that asbestos fibers of breathable size can be aligned by magnetic fields when in air or in liquid suspension. By applying light scattering to aligned particles with this method, he was able to determine quickly the identity and concentration of asbestos fibers in various samples [7]. Lilienfeld [7] used the Rayleigh-Debye-Gans (RDG) theory to determine the length of amosite fibers, this time aligned in an electric field. From a suspension of anthophyllite used by Timbrell [7], Patitsas [9] showed that it was possible to determine the modal diameter and modal aspect ratio of the particles using the same RDG theory. Moreover, he discussed the application of the RDG theory to a randomly distributed suspension. Cluff and Patitsas [10] aligned crocidolite fibers in mineral oil with an electrostatic field and used light scattering and the RDG theory to determine the modal aspect ratio and modal diameter of fibers. Lapalme and Patitsas [11,12] were interested in crocidolite and anthophyllite light scattering. They compared several theories and stated that when the fibers are aligned, the scattering from suspensions of fibers is considered using the Boundary Value Method (BVM), the Mie Substitution Theory (MST) and the RDG theory, while it is considered using the MST and RDG theories when the fibers are assumed to be randomly oriented. Stopford et al. [13] studied the real-time detection of airborne chrysotile and crocidolite using light scattering on magnetically aligned particles. The analysis first establishes if the particle is a fiber or not, and then exploits the paramagnetic properties of asbestos minerals to identify them.

From all the above researches, several fiber monitors for real-time detection have emerged, not always dedicated to asbestos. These include the FM-7400AD Real-time Fiber Monitor (MSP Corp., Shoreview, MN), the Fibrecheck HS-FC6 (Harley Scientific, UK) or the recent Asbestos ALERT (Alert Technology, UK).

Nevertheless, the above-mentioned techniques use only some aspects of the optical properties of asbestos, since, to our knowledge, the optical scattering properties (brightness and linear polarization scattering functions) of the various natures of asbestos has not been yet fully determined. To determine if instruments using scattering properties of particles can be used to detect asbestos in suspension in a medium (typically containing particles generated from a building materials), laboratory measurements of scattering functions in brightness and in linear polarization are first needed. For that purpose and to complete the database (http://www.icare.univ-lille1.fr/progra2/) used for the interpretation of remote sensing measurements of light scattered by different kinds of dust, we present here the brightness

and linear polarization scattering function of asbestos obtained in laboratory with the imaging gonio-polarimeter PROGRA2 instruments.

2. THE PROGRA2 INSTRUMENT

The PROGRA2 instruments (french accronym “PRopriétés Optiques GRains Astronomiques et Atmosphériques”, for “optical properties of astronomical and atmospherical grains”) are dedicated to the retrieval of the brightness and linear polarization scattering functions of levitating particles with random orientations [15]. Two versions are available: one in the visible and one in the near-infrared domain, called PROGRA2-Vis [16] and PROGRA2-IR [17], respectively.

The unpolarized light source is presently a halogen white lamp with a depolarizer filter and spectral filters; 525-585 and 620-680 nm for the visible domain, and 950-1100 and 1450-1650 nm for the near infrared domain. An optical fiber carries the light to the vial in which the particles are lifted by a small air injection at the beginning of the measurements [18]. The particles crossing the light beam scatter the incident light. A polarizing beam-splitter cube splits the scattered light in its two components, parallel and perpendicular to the scattering plane (I_{perp} and I_{para}), being recorded by two synchronized cameras with similar fields of view. The use of the cameras allows us to reject the images when multiple scattering could occur at the beginning of the particles’ levitation after the air injection, thus image with only single scattering are considered. Since the resolution of the cameras is ca. 20 μm per pixel, the particles cannot be individually detected. Thus, the cameras record cloud of individual particles and aggregates. The PROGRA2-IR instrument has been recently improved using CCD (Charge-Coupled Device) cameras.

The detection cameras are at fixed position, to prevent risks of misalignment when performing many measurements sessions. The vial is mounted on a rotation device and the incident light beam and the vial rotate to change the scattering angle in the 15-170° range between the measurements. Measurements are conducted at fixed angles, typically by step of 5° or 10°. Measurements of about 20 angles are necessary to retrieve the complete scattering functions.

The linear polarization P (in %) is retrieved from the two first cameras following the formula:

$$P = 100 \times (I_{perp} - I_{para}) / (I_{perp} + I_{para})$$

For the PROGRA2-Vis instrument, a third synchronized camera records the scattered light (I_{ref}) at a constant scattering angle of 90° (thus rotating with the vial) and acts as a reference camera. The brightness B (in relative units) is retrieved after the normalization of the flux recorded by the first two cameras with the flux of the third camera, following the formula:

$$B = (I_{perp} + I_{para}) / I_{ref}$$

This third camera is not available for PROGRA2-IR, thus only linear polarization functions are retrieved in the near infrared spectral domain. In the green spectral domain, the recorded flux is sometimes low at scattering angles in the 60-120° region, due to the lower sensitivity of the detectors in comparison with their sensitivity in the red spectral domain. This can affect the accuracy of the brightness retrieval because of the normalization process. Thus, we will consider in the following the brightness measurements performed only in the red domain. Finally, all scattering functions are divided with measurements obtained in the 15-20° range,

to make possible a direct comparison of the amplitude of the curves (for clarity reasons, the values of the curves are multiplied by 100). This procedure is also justified by the fact that the scattered brightness at small scattering angles for irregular grains is almost independent on the shape and the refractive index of the particles [19,20].

For safety reasons, a dedicated vial containing the sample was developed (Figure 1). The air for the particle's levitation is injected though the pipe at the middle of the device. The cellulose ester membrane filter, with a porosity of 0.45 µm in a conductive cassette above the pipe, prevents the emission of asbestos particles to the ambient air during the overpressure after the air injection.

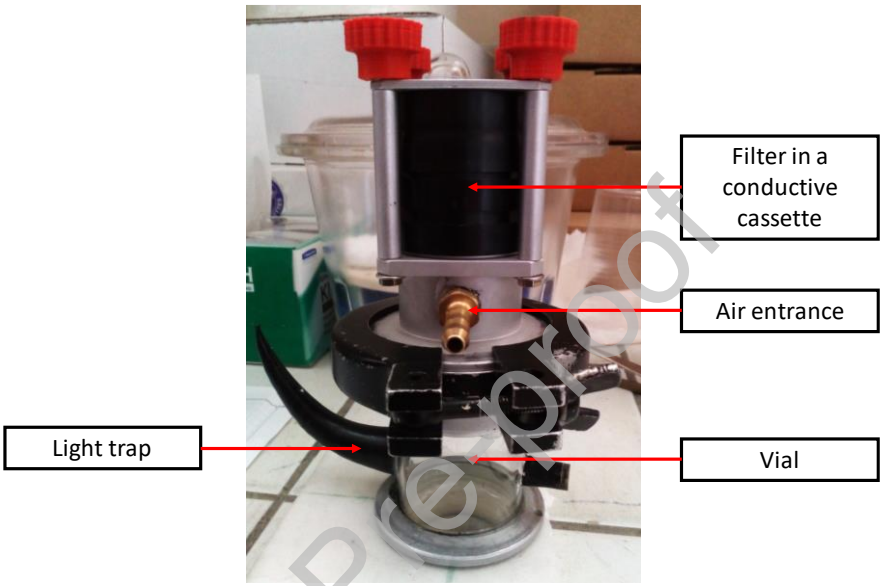

Figure 1: The vial for the levitation of the samples

3. ASBESTOS SAMPLES CHARACTERIZATION

For this study, we have selected six natural samples of asbestos from different origins, available in the BRGM (French Geological Survey) mineral collection:

- Chrysotile from Canada.
- Crocidolite from South Africa.
- Tremolite and Actinolite from France.
- Amosite from unknown origin.
- Antigorite from France. It should be noted that antigorite, of the serpentine group, is not classified as an asbestiform variety except in New Caledonia where epidemiological studies have been conducted [21].

The selected samples are as pure as possible and have been grinded in a rotary mill to obtain individual fibers or individual fiber fragments. After grinding, each sample has been analyzed by X-Ray Diffraction (XRD) in order to confirm the crystallinity, and observed by Scanning Electron Microscopy (SEM). The XRD patterns were recorded on a Bruker D8 ADVANCE Cu in a 4 to 75° 2θ range (4 to 90° 2θ for amosite), with a scanning speed of 0.03° 2θ/s and a counting time of 576 s/step, and indexed with the Diffrac.Suite EVA software. Phase quantification has been performed with the SiroQuant V.4 software. The SEM images were

acquired on a field emission gun scanning electron microscope (FEG-SEM) MIRA 3 XMU (TESCAN, Brno, Czech Republic), under high vacuum conditions with a 15 kV beam. EDS (Energy Dispersive X-ray Spectroscopy) spectra of the particles were also recorded but are not shown.

After milling, XRD shows that all samples remain crystalline (Figures 2 to 7). Chrysotile is composed of agglomerates of small particles (60 nm to 3 µm long) along with long fibers with aspect ratio (length/diameter ratio) up to 200 (130 for the fiber presented in Figure 2). For these particles, EDS exhibits a chemical composition in accordance with chrysotile (not shown). This is confirmed by XRD, which shows a 99 % pure chrysotile sample, the remaining percent being magnetite (Figure 2, also observed by SEM).

Crocidolite shows the presence of elongated particles (Figure 3) with parameters coherent with WHO's (World Health Organization) definition of fibers [1]. XRD indicates that the sample is composed of 92 % of riebeckite, the non-asbestos equivalent of crocidolite presenting the same chemical composition. Other phases such as quartz, calcite and other minor compounds are detected by XRD and SEM-EDS (Figure 3).

Tremolite is composed of agglomerates of particles of 1 µm or less along with some longer particles. According to XRD, this sample is a pure tremolite sample, as no other phase is identified (Figure 4).

The same observation is made for antigorite by XRD, indicating a pure antigorite sample. This is in accordance with SEM, which highlights the presence of particles of 5 µm or less with some agglomerates (Figure 5).

SEM observation of actinolite evidences the presence of some particles with dimensions coherent with fibers according to the WHO definition [1]. In XRD, actinolite and tremolite, the two poles of a solid solution in which Fe^{2+} replaces Mg^{2+}, are detected (Figure 6).

Amosite is composed of several elongated particles with dimensions corresponding to fibers according to WHO [1] along with agglomerates of small particles (Figure 7). XRD indicates a 98 % pure amosite, grunerite being the non-asbestos chemical equivalent of amosite.

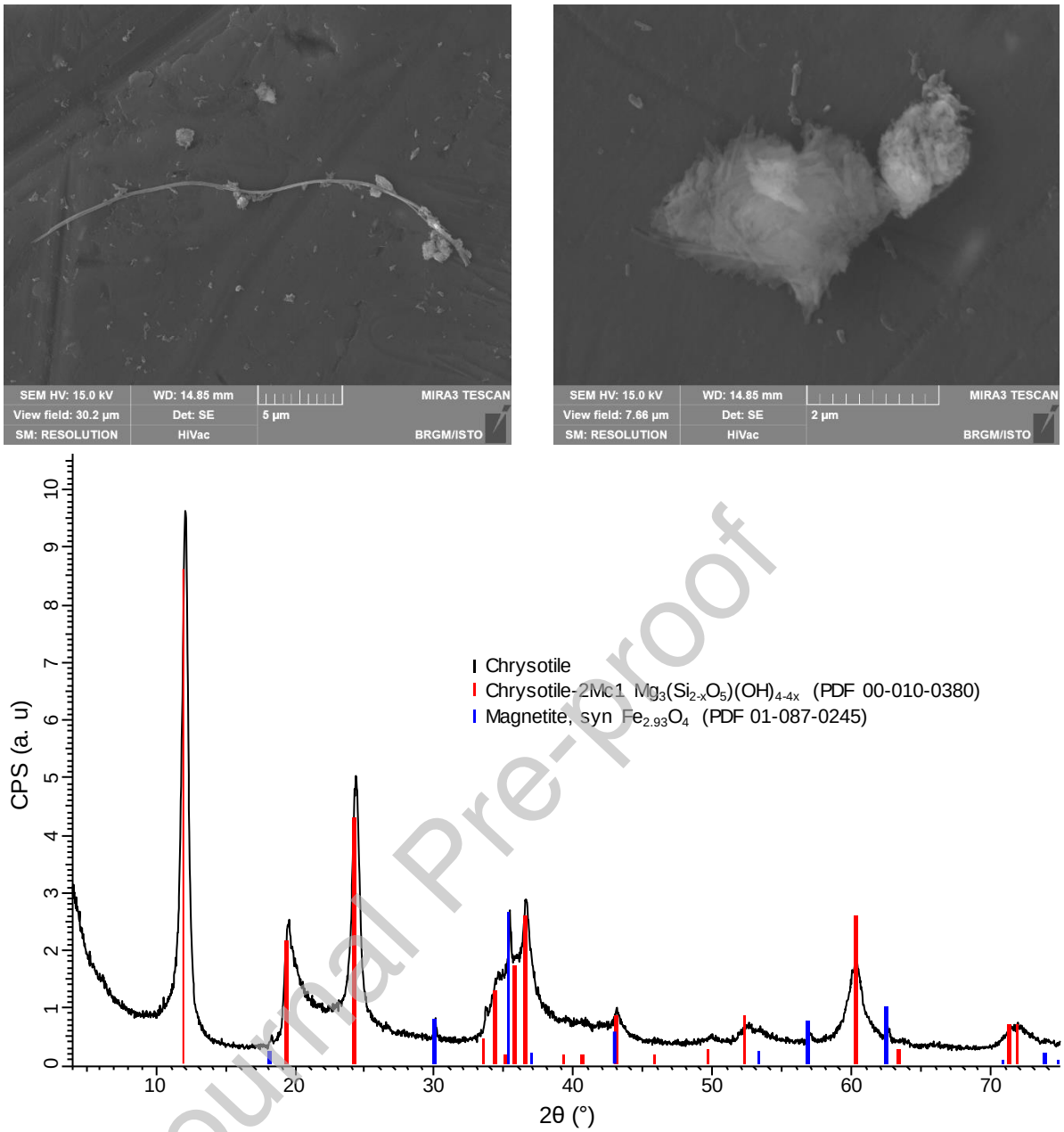

Figure 2: SEM images and XRD diffractogram of chrysotile

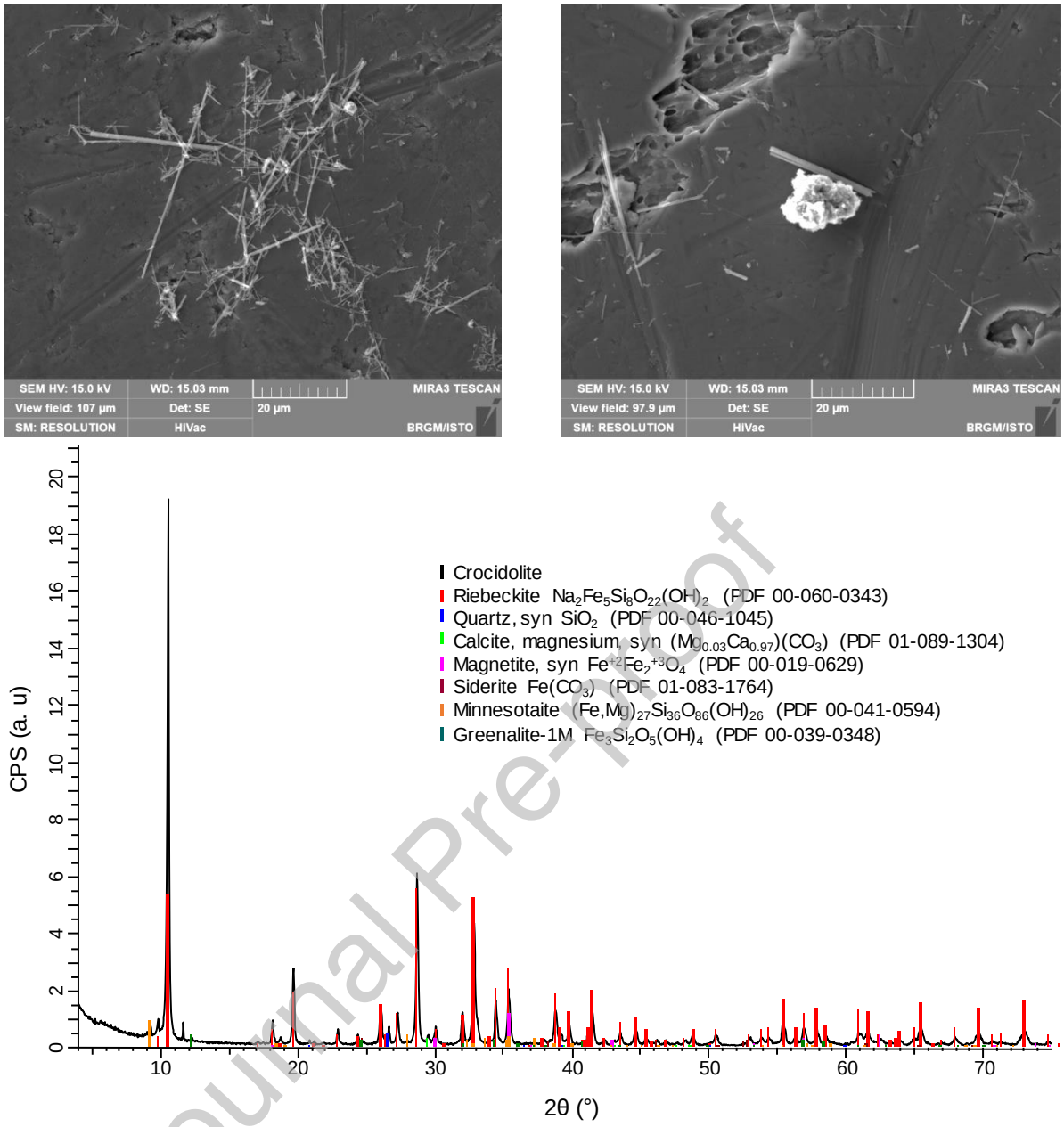

Figure 3: SEM images and XRD diffractogram of crocidolite

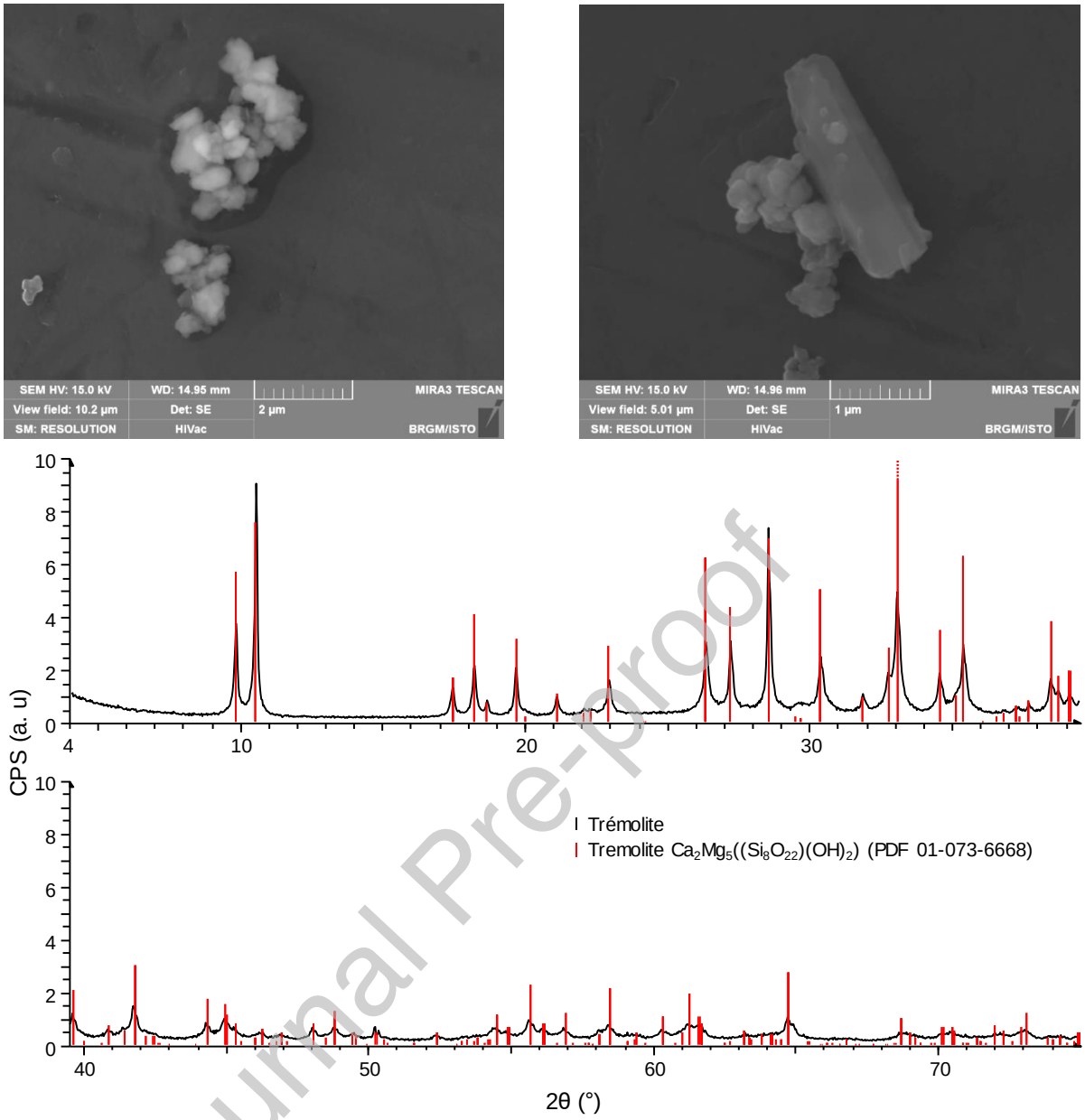

Figure 4: SEM images and XRD diffractogram of tremolite

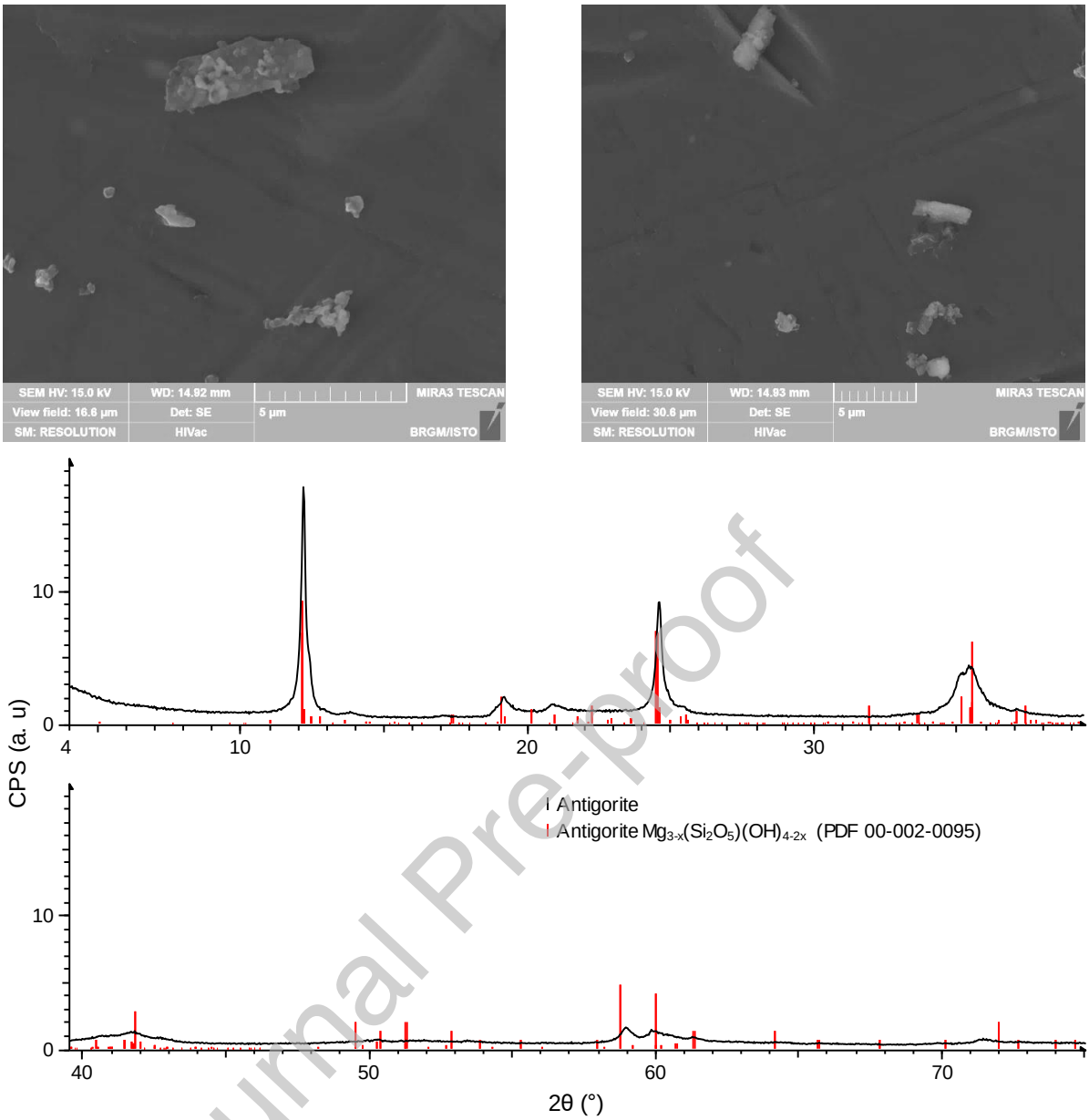

Figure 5: SEM images and XRD diffractogram of antigorite

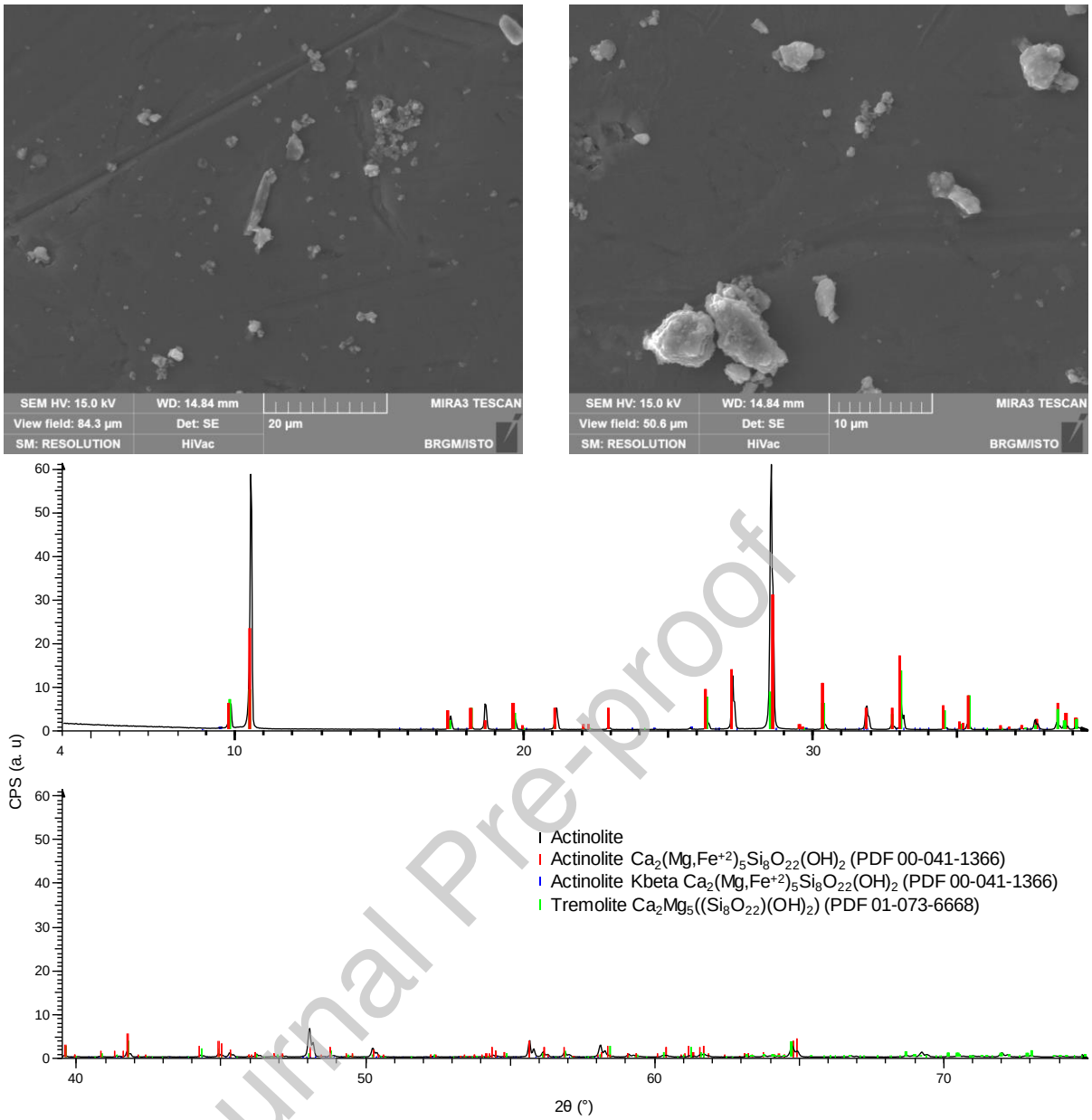

Figure 6: SEM images and XRD diffractogram of actinolite

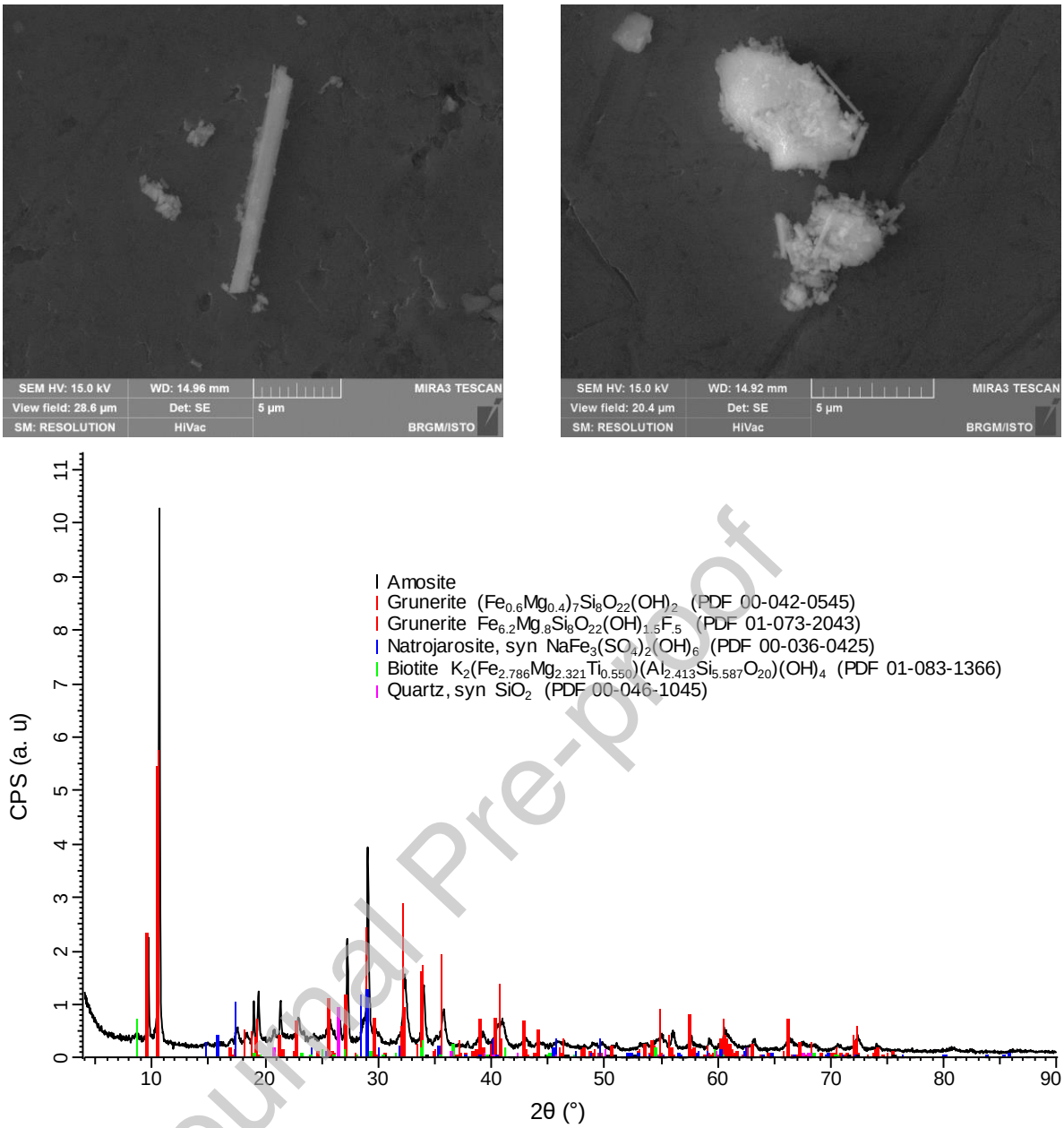

Figure 7: SEM images and XRD diffractogram of amosite

The scattering properties depend on the composition, the size, the shape and the porosity of the particles [22], but brightness and linear polarization are not always sensitive to the same parameters. Thus, we can expect different optical properties for the six samples. For comparison purpose of the optical properties of asbestos with other typical particles, additional measurements have been conducted with PROGRA2-VIS for plaster, glass wool and diesel soot. Already published PROGRA2 data will be also considered: crushed sand and clay [23], and carbon grains with monomer of 14 nm (updated form [24]). All these particles were lifted by the same method as for asbestos and were often in the form of aggregates.

4. SCATTERING FUNCTIONS

4.1 BRIGHTNESS FUNCTIONS

Figure 8 presents the brightness scattering functions obtained in the red spectral domain for the six samples of asbestos (as said before, normalized by their values in the 15-20° angle range). All the curves exhibit the same typical trend; a strong decrease at small scattering angles, a minimum of intensity in the 100-140° region and a slight increase at the large angles.

The brightness functions present some particularities, linked to the shape and internal structure of the particles. The tremolite, antigorite and actinolite curves are almost similar, while the crocidolite curve seems slightly lower for angles greater than 100°. The amosite brightness curve decreases more rapidly, followed by an almost constant brightness response in the 60-150° angle regions (considering the error bars). Finally, the chrysotile curve exhibits a strong decrease up to 80°, and the intensity in the 110-140° angle range is of ca. 3 orders of magnitude lower than the intensity at 15°, instead of about 2 orders of magnitude for the other samples.

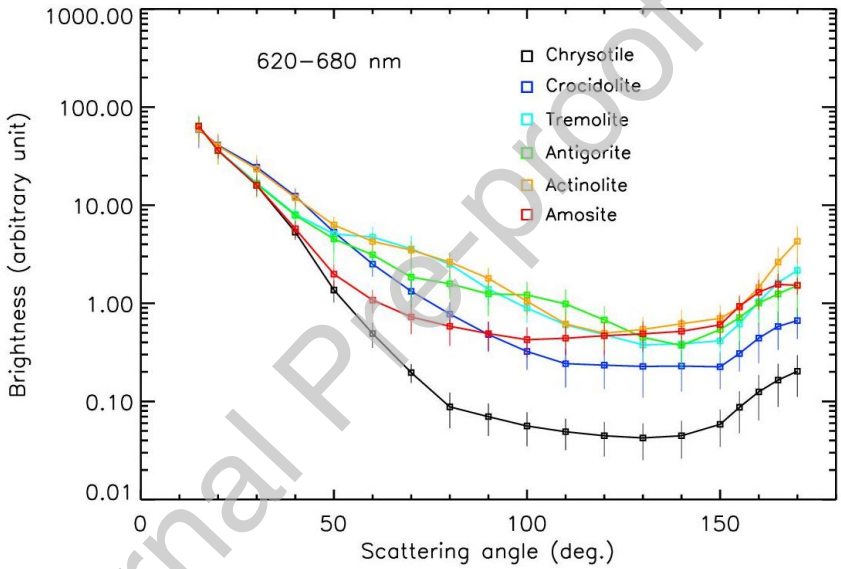

Figure 8: Brightness scattering functions in the red spectral domain

4.2 LINEAR POLARIZATION FUNCTIONS

The linear polarization functions in the visible domain are very close to zero, with a maximum of linear polarization below 10 % (Figures 9 and 10). Considering the error bars, not easy-to-detect differences can be pointed out for the different samples; nevertheless, the amosite and tremolite samples seem to produce no linear polarization.

In the near infrared domain, the linear polarization curves are higher than in the visible domain, with a maximum of linear polarization above 15 % (Figures 11 and 12). Once again, the curves are close together while the lowest one is again for the amosite.

The linear polarization slightly increases with the wavelength. The maximum of linear polarization for each sample is about twice in the near infrared than in the green spectral domain and seems to reach a “saturation” value.

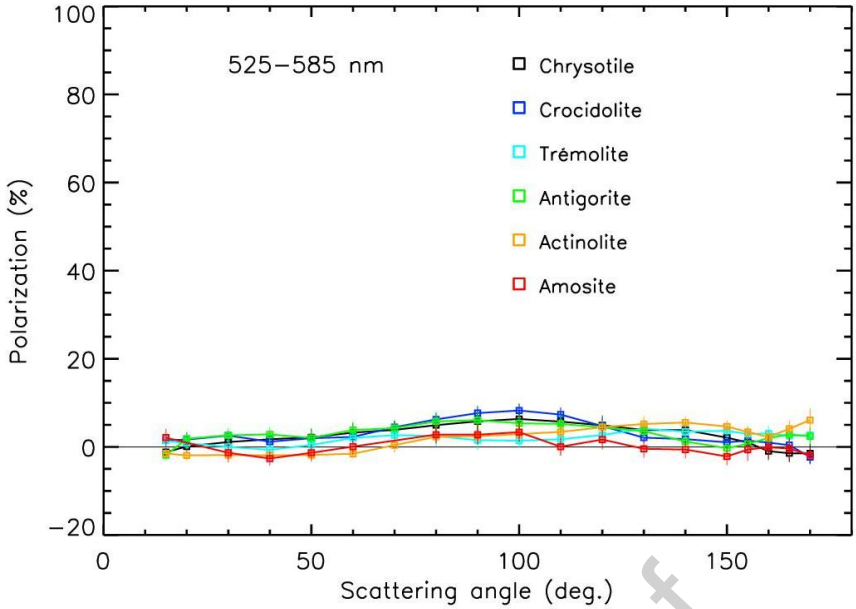

Figure 9: Linear polarization functions in the green spectral domain

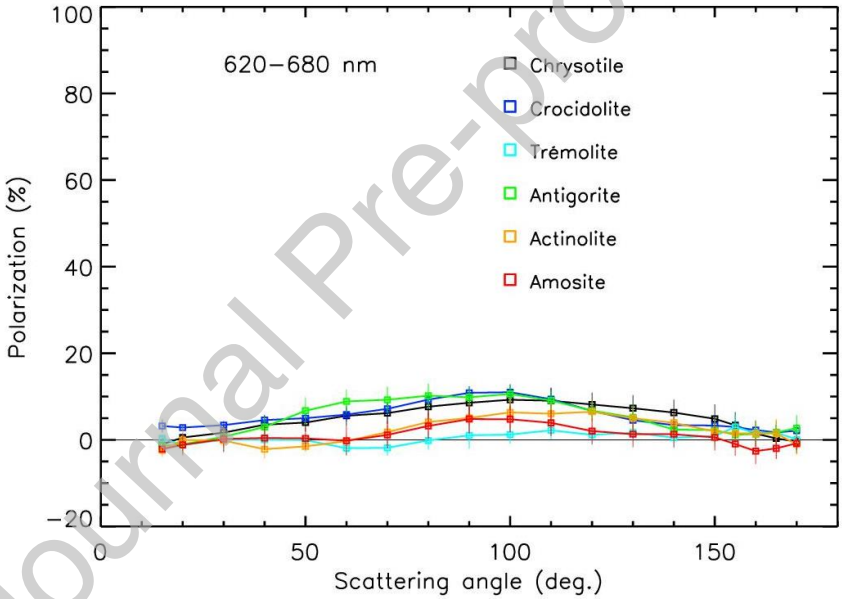

Figure 10: Linear polarization functions in the red spectral domain

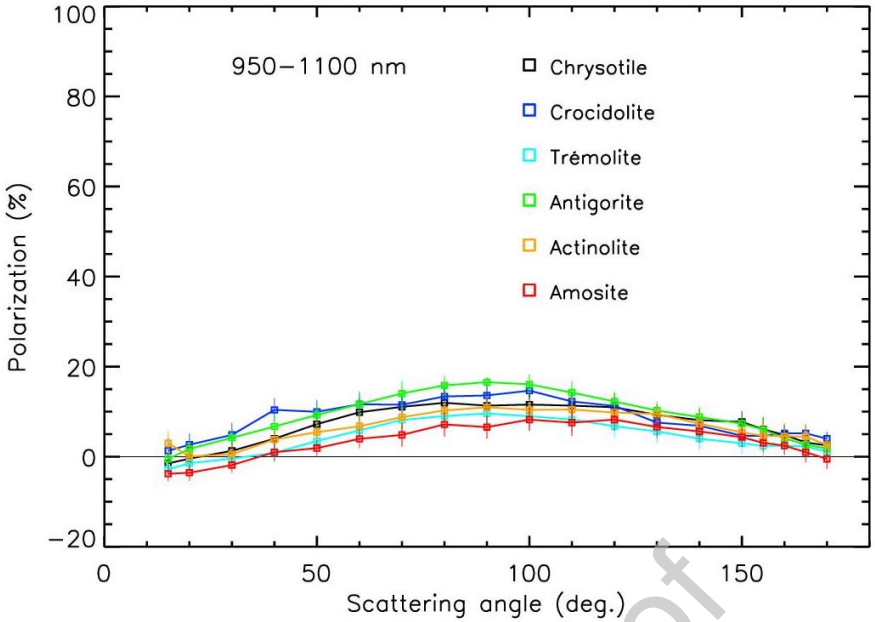

Figure 11: Linear polarization functions in the first near infrared spectral domain

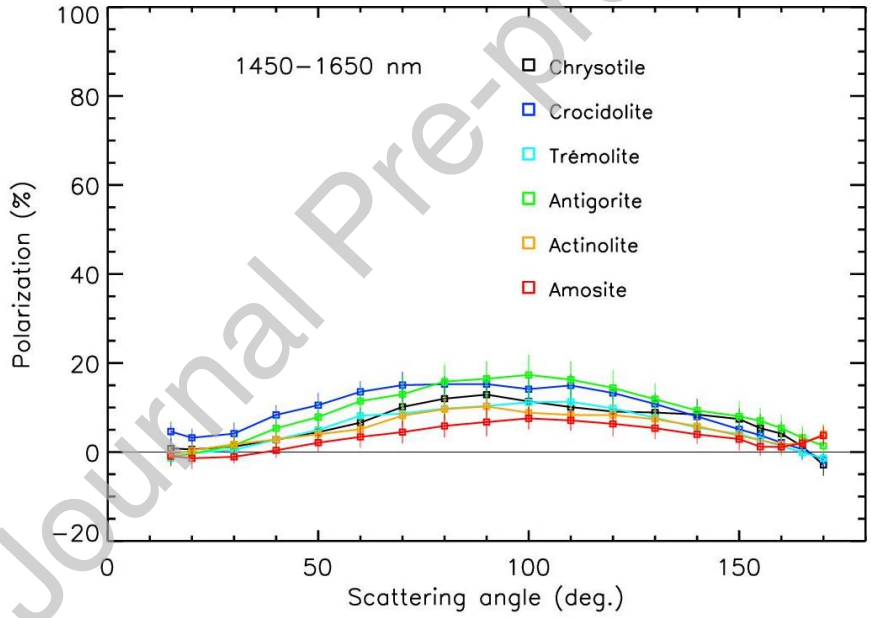

Figure 12: Linear polarization functions in the second near infrared spectral domain

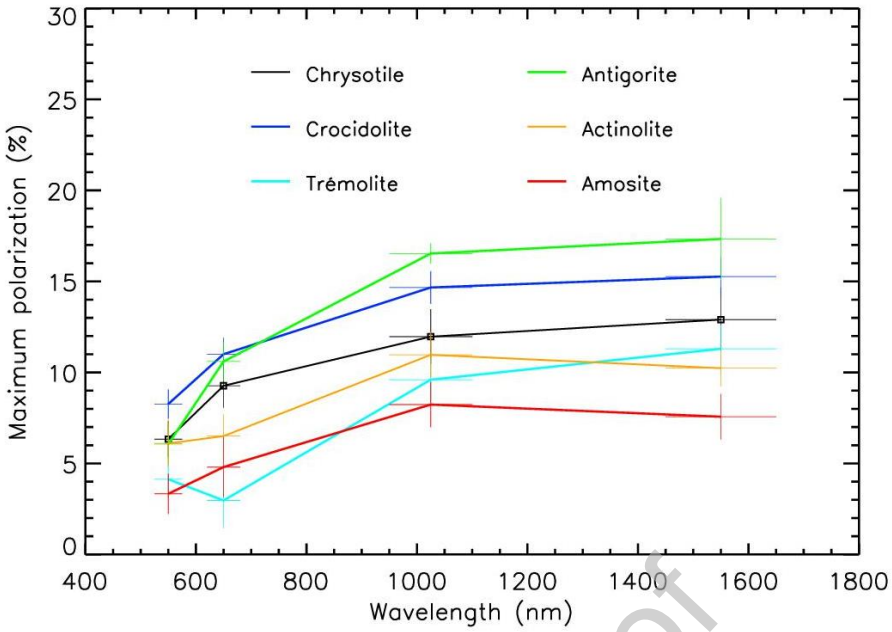

Figure 13: Evolution of the maximum of linear polarization with wavelength

5. DISCUSSION

For the comparison purpose with other natures of sample, we will consider the chrysotile and actinolite samples, which exhibits the larger and smaller amplitude in the brightness curves respectively.

Although the samples exhibit different shapes, the linear polarization values remains low, bell-shaped as usual for irregular particles, and close to those of mineral particles studied with PROGRA2-Vis (crushed sands grains, clay, grass wool, plaster) and by the "Amsterdam-Granada Light Scattering Database" team [25,26]. As a comparison, pure carbon aggregates (with monomers of 14 nm in diameter) and soot particles are presented, to illustrate that the composition and the albedo of the particles indeed dominated the linear polarization properties of the samples (Figure 14).

Nevertheless, the asbestos particle seems to exhibit a color effect that was not detected with the PROGRA2 instruments for sand particles [23], but which is similar to the one found in particular for dust particles in cometary comae [27], which are a mixture of silicates and carbonaceous particles [28]. This color effect seems also to be related to the composition of the material.

Brightness curves exhibit strong differences between the different asbestos samples and by comparison with other natures of particles here considered. For mineral particles, the less-amplitude brightness curve is obtained for the crushed sand while the strongest-amplitude brightness curve is obtained for the glass wool (which have a flat curve after 80° angle without the usual slight increase at the large angles). For carbonaceous dark particles, soot and pure carbon with monomers at least 100 nm produces the less-amplitude brightness curve while the amplitude is increasing when the size of the monomer is decreasing [24]. All asbestos curves except the chrysotile are within this "mineral region" defined within the crushed sand and glass wool region. The chrysotile is darker than the other sample in the 80-150° angle range and is included in the "carbonaceous region" defined by the soot and 14 nm

carbon particles, which is not realistic when considering the composition of the asbestos particles. These results indicate that the brightness scattering properties are also driven by the shape and the morphology of the particles. Chrysotile has a tubular shape, resulting from the rolling up of sheets [29,30] that can act as a light trap for scattering angles greater than a few tens of degrees (Figure 16).

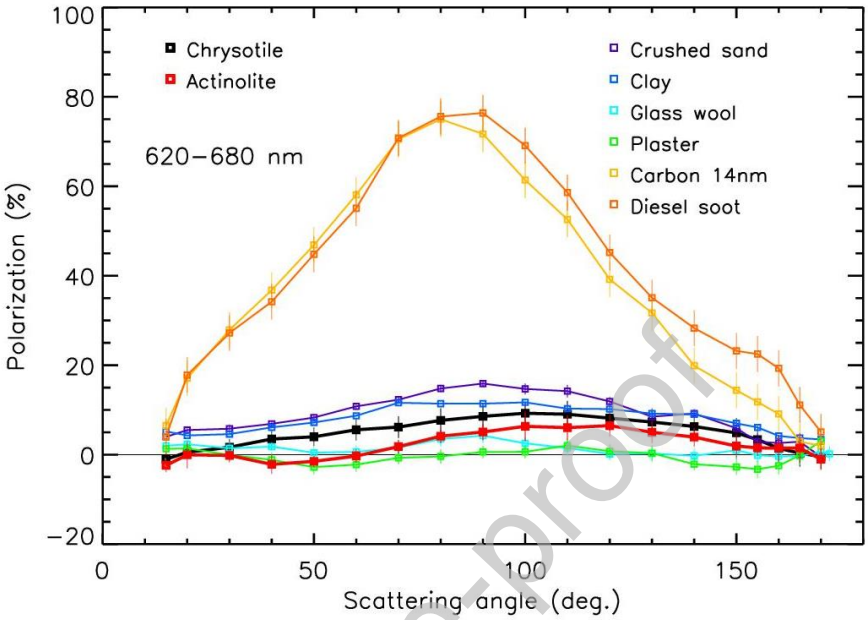

Figure 14: Comparison of linear polarization curves between asbestos and other typical particles, in the red spectral domain

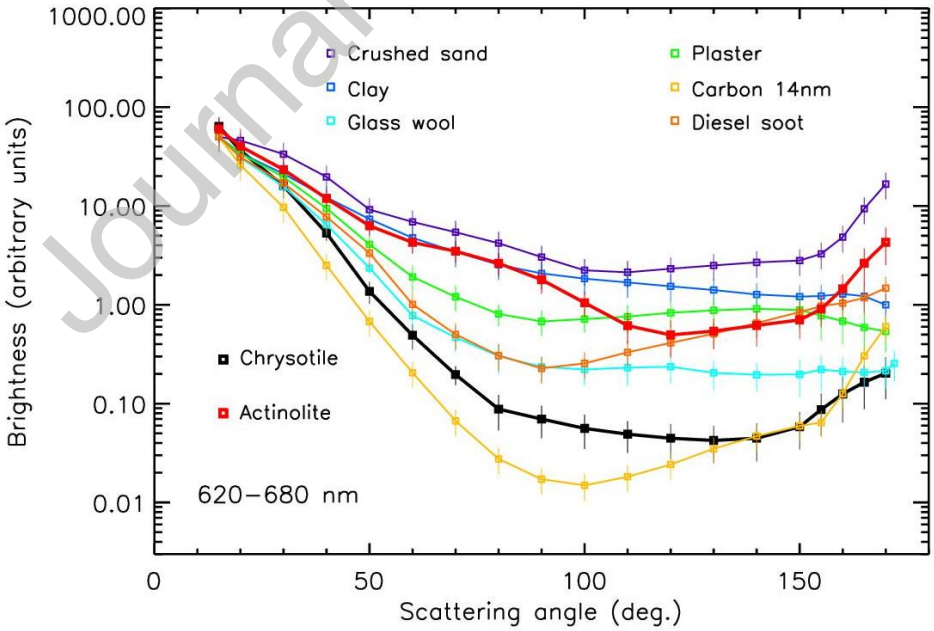

Figure 15: Comparison of brightness curves between asbestos and other typical particles, in the red spectral domain

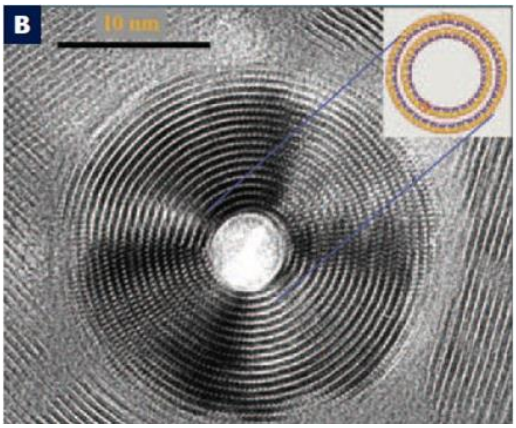

Figure 16: Chrysotile fiber structure as seen by high resolution TEM in cross section: note the hollow fiber structure of the crystal (from [31])

While being within the "mineral range", the five other asbestos can be distinguished from glass wool and plaster through their brightness curves. All the asbestos curves exhibit a significant increase for scattering angles greater than 150°, which is not the case for the glass wool and plaster. Actinolite, tremolite and antigorite have similar brightness curves that differ from the curve of glass wool for scattering angles greater than 50°, and from the plaster curve in the 50°-90° region. Crocidolite has a curve behavior different from glass wool between 50° and 90° and from plaster between 110° and 150°. Finally, the curve of amosite lies between those of these two building materials in the 50°-150° region. These first results indicate that the optical scattered properties could be used in the future to tentatively detect asbestos particles in an aerosol generated in a container from building materials. On the other hand, it seems not possible to directly detect asbestos in ambient air where particles of different origins and natures, which exhibits a large range of scattering functions, can be present simultaneously.

6. CONCLUSIONS

The PROGRA2 instruments has allowed us to document the scattering properties of six types of asbestos in the ca. 500-1600 nm spectral domain. The asbestos linear polarization curves are close together and are in the usual values of mineral particles with low linear polarization values. On the opposite, brightness scattering function exhibits a strong variability for one sample to another (as for mineral particles), and the chrysotile particles can be as dark as black carbon particles at some scattering angles, probably due to its tubular morphology that act as a light trap. Other asbestos particles can be distinguished from building materials such as glass wool or plaster through their brightness curves in some scattering angles regions; it could be possible to tentatively detect asbestos particles in a dedicated medium generated with materials coming from building activities.

Acknowledgments: This work was funded and supported by the French PRDA ("Plan Recherche et Développement Amiante"), supported by the French Ministry for the Ecological and Inclusive Transition and the Ministry for Regional Cohesion (SU 06-17-006). The authors would like to thank Raphaël Dupuy (BRGM) for careful sample preparation and Nicolas Maubec (BRGM) for XRD characterization.

AUTHOR STATEMENT

Jean-Baptiste Renard: Conceptualization, Methodology, Investigation, Funding acquisition

Cedric Duée: Conceptualization, Methodology, Investigation

Xavier Bourrat: Methodology

Hubert Haas: Conceptualization, Methodology, Investigation

Jérémy Surcin: Methodology, Investigation,

Benoit Couté: Methodology

Conflict of Interest

No conflict of interest exists.

REFERENCES

[1] WHO. Asbestos and other natural mineral fibres. Environ Health Criteria 1986; 53.

[2] NIOSH. Asbestos Fibers and Other Elongate Mineral Particles: State of the Science and Roadmap for Research. Curr Intell Bull 62; 2011.

[3] Kazan-Allen L. Asbestos and mesothelioma: Worldwide trends. Lung Cancer 2005; 49 Suppl 1:S3-8.

[4] Verkouteren JR, Wylie AG. The tremolite-actinolite-ferro-actinolite series: Systematic relationships among cell parameters, composition, optical properties, and habit, and evidence of discontinuities. Am Mineral. 2000; 85:1239-54.

[5] Verkouteren JR, Wylie AG. Anomalous optical properties of fibrous tremolite, actinolite, and ferro-actinolite. Am Mineral 2002; 87:1090-5.

[6] Timbrell V. Alignment of amphibole asbestos fibres by magnetic fields. Microscope 1972; 20:365-8.

[7] Timbrell V. Alignment of respirable asbestos fibres by magnetic fields. Ann Occup Hyg 1975; 18:299-311.

[8] Lilienfeld P. Light scattering from oscillating fibers at normal incidence. J Aerosol Sci 1987; 18(4)389-00.

[9] Patitsas AJ. Size Characterization of Asbestos Fibers Using the Rayleigh-Debye-Gans Theory. J Colloid Interface Sci 1988; 122(1):15-23.

[10] Cluff DL, Patitsas AJ. Size Characterization of Asbestos Fibers by Means of Electrostatic Alignment and Light-Scattering Techniques. Aerosol Sci Technol 1992; 17:186-98.

[11] Lapalme R, Patitsas AJ. Light Scattering by Anthophyllite-Crocidolite Asbestos Fibers, Part I: The Domain of Convergence of the EBCM Theory. Part Syst Charact 1993; 10:111-17.

[12] Lapalme R, Patitsas AJ. Light Scattering by Anthophyllite-Crocidolite Asbestos Fibers, Part II: Comparison of Various Approximate Theories with the EBCM Theory. Part Syst Charact 1993; 10:212-21.

[13] Stopford C, Kaye PH, Greenaway RS, Hirst E, Ulanowski Z, Stanley WR. Real-time detection of airborne asbestos by light scattering from magnetically re-aligned fibers. Optics Expr 2013; 21:11356-11367, 2013.

[14] Bandli BR, Gunter ME, Twamley B, Foit Jr. FF., Cornelius S.B. Optical, compositional, morphological, and X-ray data on eleven particles of amphibole from Libby, Montana, USA. Can Mineral 2003; 41:1241-53.

[15] Worms J-C, Renard J-B, Hadamcik E, Levasseur-Regourd AC, Gayet J-F. Results of the PROGRA2 experiment: an experimental study in microgravity of scattered polarised light by dust particles with large size parameter. Icarus 1999; 142:281-97.

[16] Renard J-B, Worms J-C, Lemaire T, Hadamcik E, Huret N. Light scattering by dust particles in microgravity: polarization and brightness imaging with the new version of the PROGRA2 instrument. Appl Opt 2002; 41(4):609-18.

[17] Renard J-B, Hadamcik E, Couté B, Jeannot M, Levasseur-Regourd AC. Wavelength dependence of linear polarization in the visible and near infrared domain for large levitating grains (PROGRA2 instruments). J Quant Spectrosc Radiat Transfer 2014; 146:424-30.

[18] Hadamcik E, Renard J-B, Worms J-C, Levasseur-Regourd, AC, Masson M. Polarization of light scattered by fluffy particles (PROGRA2 experiment. Icarus 2002; 155:497-08.

[19] Lurton T, Renard J-B, Vignelles D, Jeannot M, Akiki R, Mineau J-L et al. Light scattering at small angles by atmospheric irregular particles: modelling and laboratory measurements. Atmos Meas Tech 2014; 7:931-9.

[20] Renard J-B, Dulac F, Berthet G, Lurton T, Vignelles D, Jégou F. et al. LOAC, a light aerosols counter for ground-based and balloon measurements of the size distribution and of the main nature of atmospheric particles, 1. Principle of measurements and instrument evaluation. Atmos Meas Tech 2016, 9:1721-42.

[21] ANSES Saisine n° 2012-SA-0199, 2014, Evaluation of the toxicity of Antigorite (in French), https://www.anses.fr/fr/system/files/SUBCHIM2012sa0199Ra.pdf; 2014.

[22] Hovenier JW, Volten H, Muňoz OK, Van der Zande W, Waters LB. Laboratory studies of scattering matrices for randomly oriented particles: potentials, problems, and perspectives. J. Quant. Spectrosc. Radiat. Transfer 2003, 79-80:741-55.

[23] Renard J-B, Françis M, Hadamcik E, Daugeron D, Couté B, Gaubicher B. et al. Scattering properties of sand. 2. Results for sands from different origins. Appl Opt 2010; 49(18):3552-9.

[24] Francis M, Renard J-B, Hadamcik E, Couté B, Gaubicher B, Jeannot M. New studies on scattering properties of different kinds of soot. J Quant Spectrosc Radiat Transfer 2011; 112: 1766-75.

[25] Volten H, Muňoz O, Rol E, de Haan JF, Vassen W, Hovenier JW. Scattering matrices of mineral aerosol particles at 441.6 and 632.8 nm. J.Geophys Res 2001; 106(D15):17375-01.

[26] Muňoz O, Moreno F, Guirado D, Dabrowska DD, Volten H, Hovenier JW. The Amsterdam-Granada Light Scattering Database. J Quant Spectrosc Radiat Transfer 2012; 113(7):564-74.

[27] Kolokolova L, Jockers K, Gustafson BAS, Lichtenberg G. Color and polarization as indicators of comet dust properties and evolution in the near-nucleus coma. J Geophys Res Planets 2001; 106:10113-27.

[28] Levasseur-Regourd AC, Agarwal J, Cottin H, Engrand C, Flynn G, Fulle M. et al. Cometary dust. Space Sci Rev 2018; 214:64-19.

[29] Bonneau L, Suquet H, Malard C, Pezerat H. Studies on surface properties of asbestos : I. Active sites on surface of chrysotile and amphiboles. Envir Res 1986; 41:251-67.

[30] Martin CJ, Phillips VA. The texture of chrysotile asbestos in relationship to mechanical properties. Mater Sci Eng 1977; 30:81-7.

[31] Williams-Jones AE. Mineralogically, What is Asbestos and How Does it Form? https://slideplayer.com/slide/4644005/.